PANAMGEO CHILE 2024
17th PAN-AMERICAN CONFERENCE ON SOIL MECHANICS AND GEOTECHNICAL ENGINEERING | 2nd LATIN-AMERICAN REGIONAL CONFERENCE OF IAEG
LA SERENA • CHILE / NOVEMBER 12 - 16, 2024

Proceedings of the 17th Pan-American Conference on Soil Mechanics and Geotechnical Engineering (XVII PCSMGE), and 2nd Latin-American Regional Conference of the International Association for Engineering Geology and the Environment (IAEG), La Serena Chile, 2024.

Numerical Analysis of Anchor-Chain-Soil Interaction under Operational Loading on Floating Offshore Wind Turbines

Análisis Numérico de la Interacción entre el Ancla, la Cadena y el Suelo bajo Carga de Servicio en Turbinas Eólicas Flotantes Mar Afuera

Duy A. Dao & Jürgen Grabe

Institute of Geotechnical engineering and Construction Management, Hamburg University of Technology, Germany, duy.anh.dao@tuhh.de

ABSTRACT: Floating offshore wind turbines (FOWTs) are kept in position by mooring lines that are attached to anchors. When designing FOWTs, anchoring points are typically assumed to start at the mudline; however, anchors require deep embedment into the seabed for appropriate stability. Furthermore, the mooring chains of deeply embedded anchors experience movement, possibly leading to reduced soil resistance. Prevailing two-dimensional analysis of FOWTs offer limited insight into the complex interactions between anchor chains and the seabed. This study introduces a three-dimensional model that includes the anchor, in this case the Stevshark Mk5, and the anchor chain embedded as an inverse catenary. It is designed to investigate soil stress and deformation resulting from anchor chain ploughing. The numerical force-controlled simulations apply the FEM method integrated with the coupled Euler-Lagrange approach (CEL) to accommodate large deformations. A hypoplastic framework is used for realistic soil modeling and compared against the Mohr-Coulomb model, a numerical soil-structure interaction model. The results reveal notable differences regarding stress distribution in comparison to simplified solutions that only use a point mass for the anchor structure and only the Mohr Coulomb model. They also show a large impact when varying the void ratio and anchor line angle. Overall, this model serves as a promising base for robust numerical models to better understand the complex anchor-chain-soil interaction.

KEYWORDS: anchor chain, floating offshore wind turbine (FOWT), offshore geotechnics, offshore foundations, CEL

1 INTRODUCTION

On land, available space for wind turbines with fast enough and steady wind is limited. In contrast, wind speeds are higher and more constant in regions far from the coast as the water depth increases. However, offshore wind turbines only present as an economically feasible option for water depths less than 60 m, as the forces acting on the system require cross-sections that become exponentially too large. With floating mooring systems, it is possible to install FOWTs in high water depths, where electricity generation will be efficient and economically worthwhile. In these systems, the FOWT is held in place by a mooring line attached to an anchor installed in the seabed.

Conventional models of anchoring systems typically assume that the anchor remains fixed in position, as indicated in studies by Vivatrat et al. (1982), Degenkamp and Dutta (1989), Neubecker and Randolph (1995), Xiong et al. (2016), and O'Neill et al. (2018). Contrarily, Kwa et al. (2022a, 2022b) examine the impact of operational load on the deformation and resistance of a plate anchor including a chain that originates at the mudline but is not embedded. Maitra et al. (2022) explore the anchor-soil interaction during installation using a two-dimensional model.

The complex interaction between the soil and an anchoring system, which can lead to soil failure, necessitates a fully three-dimensional simulation to accurately capture the deformation process. This requirement has been underscored in research by Wang et al. (2010) and O'Neill et al. (2003). Extending this approach, Dao and Grabe (2022), Dao et al. (2023), and Dao and Grabe (2024) have presented numerical 3D models that detail large movements of the anchor during installation and dragging phases. For the system's operational state, studies by Zhao and Liu (2016), Sun et al. (2019), and Dao et al. (2022a) have developed 3D models using the coupled Euler-Lagrange (CEL) approach in Abaqus to analyze anchor chain behavior, a methodology again applied here.

Zhao and Liu (2016) modeled the anchor chain's transition from a vertical orientation at the shackle to a horizontal position at the seabed, a scenario typical for pile-installed and heavyweight anchors. Building on this framework, Sun et al. (2019) extended the model to further evaluate the normal and frictional resistance of the soil against the anchor chain. These studies differ in regard to the traditional inverse catenary shape typical of DEAs. Moreover, they simplify the anchor as a fixed point, neglecting its mass and potential displacement. Conversely, Dao et al. (2022a) modeled the anchor as a movable mass point, demonstrating that simplifying the point to either a fixed or loose support is insufficient. However, all previous CEL simulations considering the operational load of the anchoring system have employed either linear-elastic or elastoplastic simplifications of the soil model, which are not able to realistically reproduce the response of the anchoring system under cyclic load.

In this contribution, a numerical CEL model was created to investigate the behavior of an anchoring system for floating offshore wind turbines under cyclic load. The numerical investigation focused on a section of the mooring system embedded in the seabed, as illustrated in Figure 1, and features a chain attached to a fully modeled anchor that is movable.

2 NUMERICAL METHOD

Geotechnical problems are often modeled as initial boundary value problems and addressed using numerical methods such as the finite

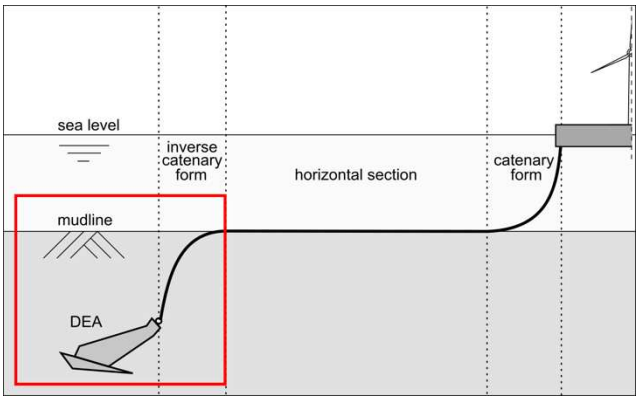

Figure 1. Non-scale design concept of an anchored FOWT.

element method (FEM). FEM discretizes the solution domain into a mesh of finite elements with shared nodes, where the problem's solution is approximated (Zienkiewicz et al., 2005). The geomechanical behavior of soils in FEM can be represented through different frameworks, notably the Lagrangian and Eulerian approaches, illustrated in Figure 2.

The Lagrangian method pins the computational mesh to the material, enabling precise delineation between distinct materials but is less suitable for large deformations due to potential mesh distortion and consequent numerical instability. Conversely, the Eulerian method maintains a fixed grid through which the material flows, effectively handling large deformations without mesh distortion but at the risk of material property diffusion across stationary nodes.

To leverage the strengths of both, the coupled Euler-Lagrange (CEL) method combines them, applying the Lagrangian approach to structures and the Eulerian approach to zones of expected significant deformation (Noh, 1964; Benson, 1992). Commercially available in FEM software such as Abaqus/Explicit (Dassault Systèmes, 2020), the CEL method has demonstrated efficacy in simulating complex offshore scenarios, as validated by studies (Kim and Hossain, 2015; Bienen et al., 2020; Stapelfeldt et al., 2020; Dao et al., 2022b; Dao and Dicke, 2024).

3 NUMERICAL MODEL

The numerical simulations focus on the behavior of an anchor chain attached to a DEA, as it is currently the most frequently used anchor type for FOWTs. The chosen load time series is taken from Kwa et al. (2023a) and is based on the IEC design load case for the operational load scenario DLC 1.12. From this load series, the maximum tensile force acting on the anchor was determined and a required ultimate holding capacity UHC = 390 t was selected and the dimensioning of the anchor and its chain was carried out, according to Vryhof (2018). For the anchor chain, it was decided to use an anchor chain consisting of chain links modeled as cylindrical rigid bodies. Chain link connections were provided between the chain links to transfer axial forces. The behavior under cyclic load was investigated using the fully modeled DEA. In addition, the dimensions of the soil model were determined using the chain link dimensions and the height of the anchor.

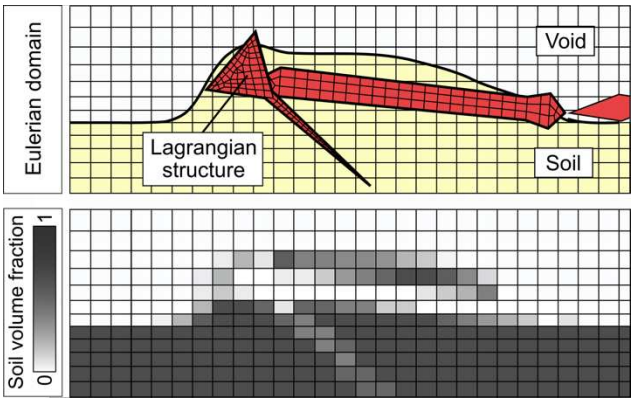

Figure 2. Schematic 2D representation of anchor penetration process using the CEL method (top), and the corresponding soil filling degree in correspondence with the resulting soil deformation (right).

3.1 *Modeling of the mooring System*

At the beginning of the simulation, the anchor chain links are positioned so that they form an inverse catenary shape. At its deepest point, the chain is attached to the DEA model. Figure 3 presents the setup of the model.

3.1.1 *Modeling of the chain links*

The anchor chain in the simulation is represented by a sequence of uniformly sized cylindrical rigid bodies, characterized by segment length l_s, diameter d_s, and the spacing between adjacent segments s_s, according to Sun et al. (2019). They are meshed using 16 linear hexahedral elements of type C3D8R. Figure 5 depicts the correlation between an actual steel warp and its abstracted representation in Abaqus, where each warp unit is simplified as a cylindrical rigid body connected by a distance s_s. Due to the system's symmetry, only half of each segment is modeled, bisected along the chain axis. Given the substantial stiffness of steel relative to soil, it is reasonable to assume minimal impact of chain strain on the simulation results. Thus, the chain links are modeled as rigid bodies. Each segment is assigned a mass of 55.7 kg, aligning with the buoyancy density of steel.

3.1.2 *Chain configuration*

In this study, the interconnection of chain segments is simulated using link connectors, which are designed to transmit axial forces while maintaining a constant length of the connecting section. The chain link positions are calculated analytically using the equations provided by Neubecker and Randolph (1995). This configuration is determined by specifying the anchor line angle at the anchor shackle, denoted as ϑ_a. Point coordinates are calculated for the specific angle of ϑ_a at the anchor shackle. These coordinates are subsequently utilized in the modeling of the chain segments. Figure 4 presents the whole construction procedure for the embedded inverse catenary chain.

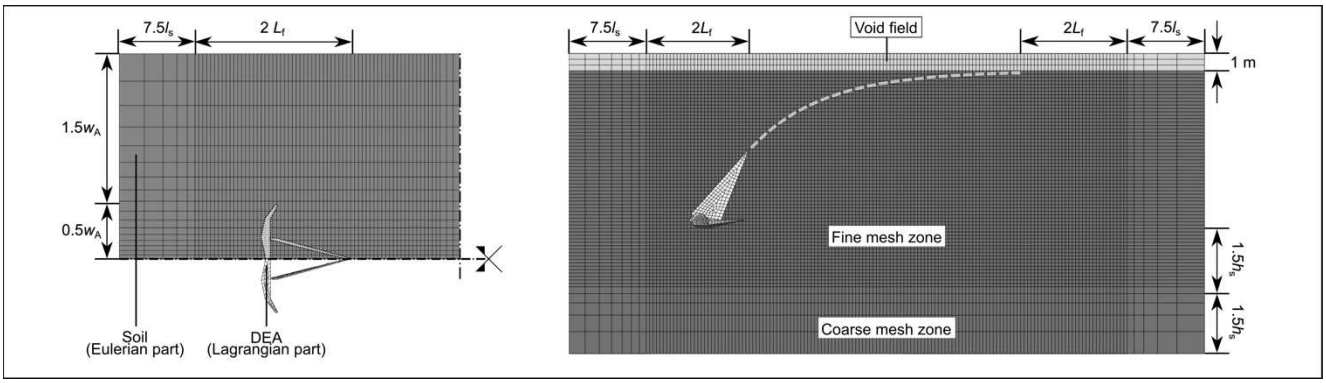

Figure 3. Top view of the model (left) and side view of the model (right).

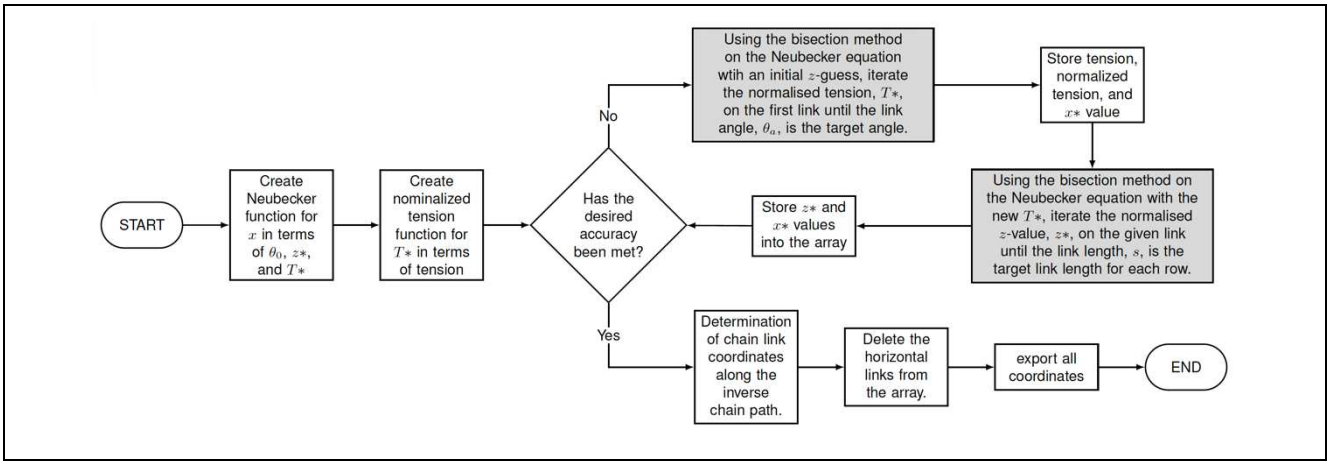

Figure 4. Flow chart of the construction procedure for the embedded inverse catenary chain.

3.1.3 *Anchor modelling*

The DEA model is based on an 8 t Stevshark Mk5 anchor from Vryhof and defined as a rigid body, with the center of mass serving as reference point *R*p, according to Fig. 6. Its dimensions are listed in Table 1. The anchor model's mesh consists of 1358 linear quadrilateral R3D4 elements and 117 linear triangular R3D3 elements.

3.2 *Eulerian Soil and Void Domain*

The soil is modeled as an Eulerian cuboid to accommodate large deformations. To prevent boundary condition interference, sufficiently wide enough distances between the structural elements and the model boundaries are maintained, according to Fig. 3. An additional 1 m high Eulerian body is introduced above the mudline to serve as a void space, allowing soil expansion during deformation. The anchor chain is implemented using a 'wished-in-place' approach, aligning chain segments according to Neubecker and Randolph (1995) at the simulation's start, thus omitting stresses from the anchor installation. Recesses are created in the soil body for the chain, ensuring initial embedding and distinct separation between Eulerian and Lagrangian bodies. Mesh refinement is concentrated in high-stress, high-deformation areas, particularly around the anchor chain. The soil mesh, made of EC3D8R hexahedral elements, is finer near the chain and coarser further away, totaling 183,464 elements.

The Mohr-Coulomb model and the hypoplastic model were used for the numerical calculations. The parameters for the Mohr-Coulomb model are detailed in Table 2. The 50 % secant modulus was used for the stiffness in the Mohr-Coulomb model, based on triaxial tests presented in Chow et al. (2019), The Poisson's ratio ν and the cohesion c were estimated based on typical values for sand. The friction angle φ was taken from Chow et al., 2019. The dilation angle was approximated using

$$\psi \approx \varphi - 30\,°. \tag{1}$$

Hypoplasticity by von Wolffersdorff, P.-A. (1996) is an advanced incrementally non-linear constitutive model that reflects the pressure and density-dependent behavior of soil. This model has been validated across a range of geotechnical issues through numerous single and finite element simulations. When integrated with the intergranular strain concept by Niemunis and Herle, (1997), sand hypoplasticity effectively predicts the degradation of small strain stiffness and the impacts of cyclic load. Machaček et al. (2022) determined the hypoplastic parameters for UWA sand which are applied for modeling. A list and description of the required parameters and laboratory tests to determine the substance parameters can be found in Herle and Gudehus (1999), Dao and Banduch (2023) and Cerek et al. (2024).

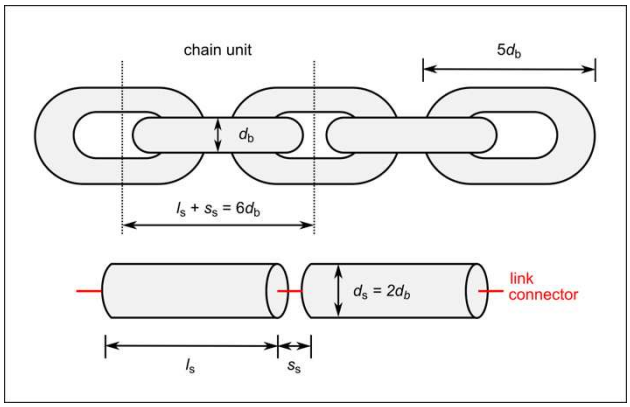

Figure 5. Chain link simplification, adapted from Sun et al. (2019)

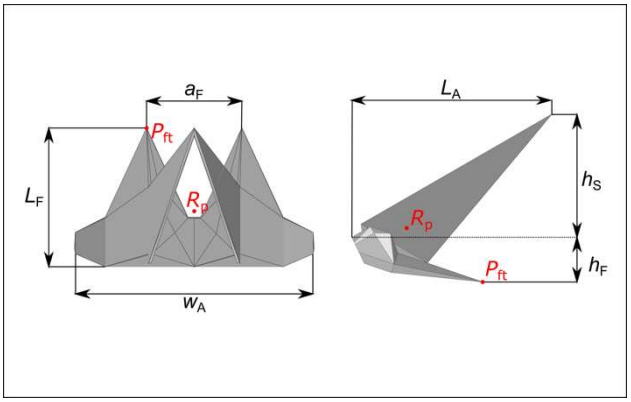

Figure 6. Plane view (left), side view (right) of simplified DEA model and locations of reference point R_p and fluke tip P_{ft}.

Table 1. Anchor model dimensions.

Dimension	a_f	h_f	h_s	L_a	L_f	w_a
Length (m)	2.15	0.47	2.63	5.16	3.41	5.56

Table 2. Applied Mohr-Coulomb parameters.

Quantity	Magnitude	Unit
specific weight γ'	1.67	t/m3
friction angle φ'	33.1	°
Young's modulus E	104800	kN/m2
Poisson's ratio v	0.3	-
cohesion c	0	kN/m2
dilation angle ψ	3.1	°

Table 3. Applied hypoplastic parameters.

Parameter	Value	Unit	Description
γ'	1.67	kN/m^3	specific weight
φ_c	29.56	°	Critical friction angle
h_s	54.86	MPa	Granular stiffness
n	0.2436	-	Exponent
e_{d0}	0,442	-	Minimum void ratio
e_{c0}	0.810	-	Maximum void ratio
e_{i0}	0.932	-	Critical void ratio
α	0.2584	-	Exponent
β	0.2256	-	Exponent
m_T	1.6	-	Factor
m_R	3.2	-	Factor
R_{max}	2×10^{-4}	-	Constant
β_χ	0.03	-	Exponent
χ	1.5	-	Exponent

3.3 *Load history and boundary conditions*

The operational design load case DLC 1.12 from the IEC was considered to analyze the influence of different loads on the wind turbine and its anchoring system from wind, waves and currents. The data used on the tensile forces acting on the mooring system were taken from Kwa et al. (2023a). The maximum tensile force depending on the load case was used for the subsequent dimensioning of the model components. Figure 7 (top) displays the load time series, as extracted from Kwa et al. (2023a), with the selected time frame delineated by a red box. Preceding this time frame, a linearly increasing load application is introduced, as depicted in Figure 7 (bottom). When selecting the section of the cyclic load used, care was taken to ensure that the maximum tensile force was part of the selected simulation time. Due to the existing symmetry of the model, only one half of the numerical model was considered in the simulation in order to reduce the calculation time. Therefore, the acting cyclic tensile forces were also halved.

The load history used for the simulation consisted of the initial phase, the preparation phase and the load phase, according to Table 4. In the initial phase, the initial boundary conditions and the stress state in the soil were generated. Initially, the simulation generates the soil's stress state, arising from its self-weight. This initial state is characterized by an effective vertical stress, denoted as $\sigma_{v,0}$, and an initial effective horizontal stress, $\sigma_{h,0}$, calculated as the vertical stress multiplied by the earth pressure coefficient K0. K0, dependent on the soil's friction angle φ, is estimated using Eqn 1.

$$K_0 = 1 - \sin\varphi \tag{2}$$

The anchor chain is then positioned under the 'wished-in-place' assumption, meaning it is in place at the start of the phase without considering stresses and deformations from the installation process. By neglecting the installation process, a homogeneous soil was initially present in the simulations carried out here. In addition, no soil resistance was generated in front of the anchor and the compaction caused by the installation process of the anchoring system was not taken into account. Due to the lack of soil resistance, double gravity was assumed for the further simulations and the load for which the anchoring system was designed was reduced to 1/100 of the load.

The second step, the gravitational phase, activates the gravitational force acting on the system as 9.81 m/s².

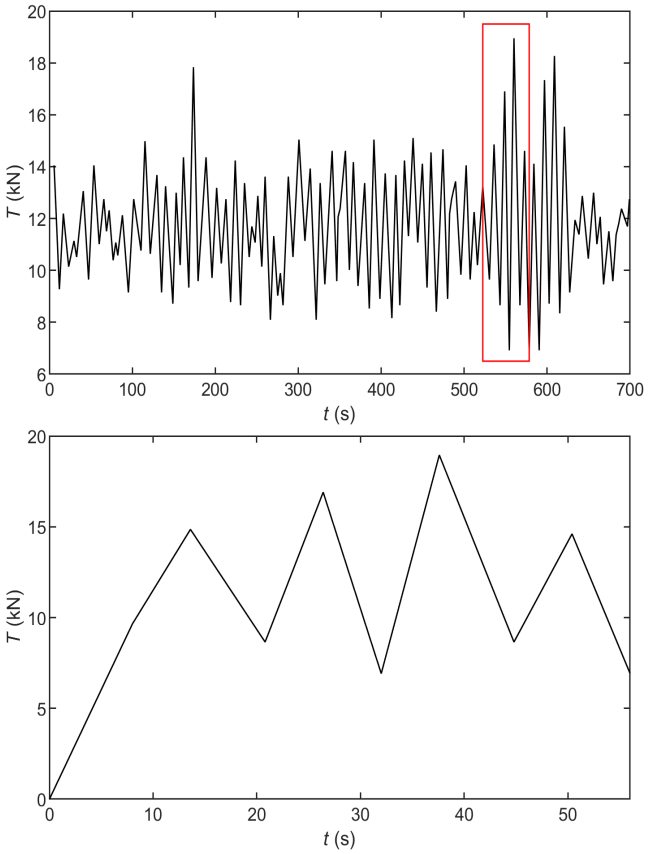

Figure 7. Force curve of IEC load case DLC 1.12 from Kwa et al 2022 (top) and selected section of the force curve for the simulations (bottom).

Table 4. Simulation steps.

Step	Phase	Description	t (s)
1	Initial phase	Initial boundary conditions activation	-
2	Gravitational phase	Activation of gravity	4
3	Dragging	Activation of tensile load	56

Table 5. List of conducted simulations.

No.	Constitutive model	Anchor line angle ϑ_a (°)	Void ratio e (-)
1	Mohr-Coulomb	45	-
2	Hypoplasticity	30	0.656
3	Hypoplasticity	45	0.656
4	Hypoplasticity	60	0.656
5	Hypoplasticity	80	0.656
6	Hypoplasticity	45	0.525
7	Hypoplasticity	45	0.787

In the final phase, a tensile load is applied to the anchor chain. The load is applied to the reference point on the chain link nearest to the mudline.

For all simulations, the initial state of horizontal stresses remains approximately constant. Figure 8 illustrates a homogeneous stress distribution across the soil, defined by the earth pressure at rest. For visualization, the stresses are grouped into distinct ranges, starting at zero at the mudline and increasing with depth.

4 RESULTS AND DISCUSSION

To investigate the impact of various parameters on the behavior of soil and anchoring systems under cyclic load, several simulations were conducted. These simulations varied in terms of the constitutive model, anchor line angle ϑ_a, and initial void ratio e_0, as summarized in Table 5. The results were evaluated by examining the horizontal stress states in the soil, as well as the horizontal and vertical displacements of the anchor throughout the loading period.

4.1 *Impact of the constitutive model and anchor model*

Figure 8 displays the initial position of the anchor chain and the horizontal stress states for two simulations: Simulation 1 employing the Mohr-Coulomb model, and Simulation 2 using the hypoplastic model. Figure 9 illustrates the configuration of the anchor chain and the horizontal stress states following operational loading. The comparison between the Mohr-Coulomb and hypoplastic simulations revealed minor differences in the level of horizontal compressive stresses in the soil. Following cyclic loading, the area near the anchor chain exhibited increased stresses in both models; however, these stresses were higher in the Mohr-Coulomb simulations. Additionally, a reduction in stress was observed around the anchor in areas of the soil modeled using the hypoplastic approach.

The Mohr-Coulomb model assumes constant soil stiffness throughout the test duration, while the hypoplastic model accounts for increased stiffness during reloading under cyclic conditions. This omission in the Mohr-Coulomb model results in significantly larger permanent deformations.

Figure 10 illustrates the displacement of the anchor fluke tip. In the Mohr-Coulomb model, displacements were positive, moving in the direction of drag and upwards toward the mudline. Conversely, the hypoplastic model registered negative vertical displacements, indicative of sinking. These negative displacements, considered realistic, reflect the combined effects of dead weight, gravity, and soil settlement, suggesting that gravity had a more significant impact on the anchoring system than the tension load.

The model by Dao et al. (2023) also employs the Mohr-Coulomb model and demonstrates an increase in stress directly beneath the chain. Figure 11 illustrates the final state of one of these simulations, where the anchor is represented by a small cube. In terms of stress distribution, a pressure area develops below the chain segments, spanning the entire length of the chain. This area of pressure is most pronounced in the lower third of the chain, where the structure shears through the soil most intensively.

Furthermore, the soil that has been disturbed by the chain initially exhibits lower stress compared to soil at the same elevation further from the chain, suggesting soil loosening. However, the Mohr-Coulomb simulations conducted in this study reveal a more pronounced stress state around the anchor, which is absent in the simulations by Dao et al. (2023).

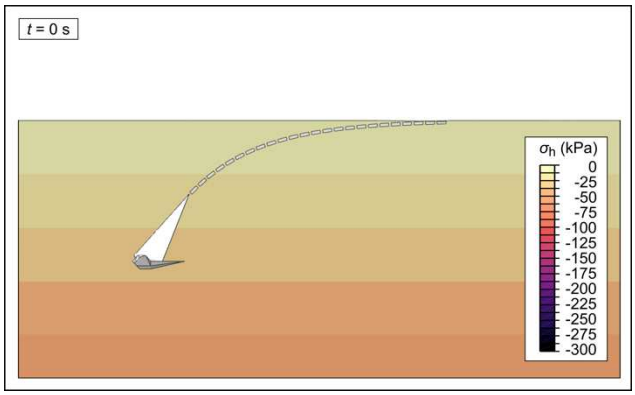

Figure 8. Configuration of anchor chain and stress state (in kPa) in initial state.

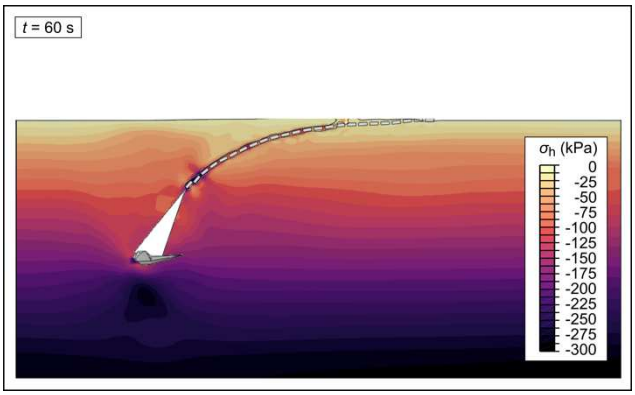

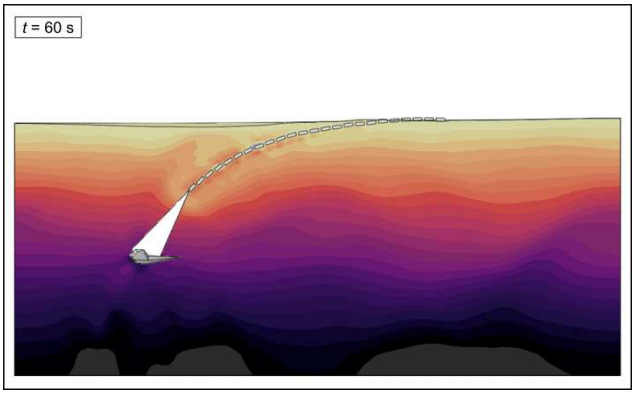

Figure 9. Configuration of anchor chain and stress state (in kPa) of the soil after loading for Mohr-Coloumb (top) and Hypoplasticity-based (top) simulations 1 and 2.

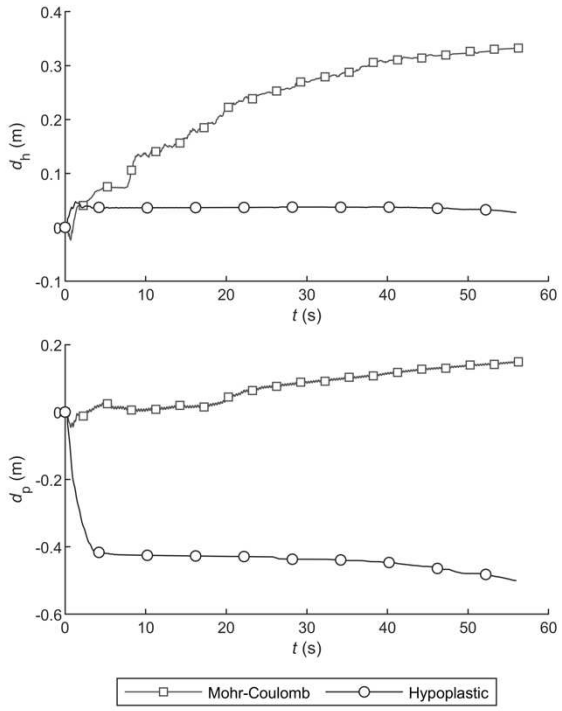

Figure 10. Horizontal (top) and vertical (bottom) displacement d_h and d_p of the anchor fluke tip P_{ft} during loading for different constitutive models.

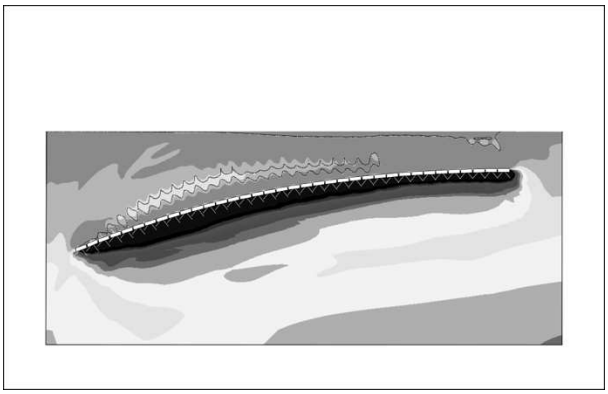

Figure 11. Configuration of anchor chain and stress state (in kPa) of the soil after pulling (fixed anchor point), for different anchor models by Dao et al. (2023).

In all simulations, the chain retains an inverse catenary shape following cyclic loading. The use of a separate body for modeling, as implemented by Dao et al. (2023), along with the application of the Mohr-Coulomb constitutive model, are both found to be unsuitable. The Mohr-Coulomb model in particular does not realistically replicate the response to cyclic loading, showing significantly less resistance compared to soil modeled with hypoplasticity.

These factors, combined with the absence of a structural surface, lead to an overestimation of horizontal displacement. Consequently, employing a cubic replacement anchor to investigate the behavior of the anchoring system should be limited to providing only a rough estimate.

4.2 *Impact of anchor chain angle*

At the conclusion of cyclic loading, simulations 2 to 5 exhibited similar stress distributions across the soil body when the angles were varied. Specifically, a steep angle of 80 ° in these simulations resulted in localized stress formation directly above the anchor, see Fig. 12.

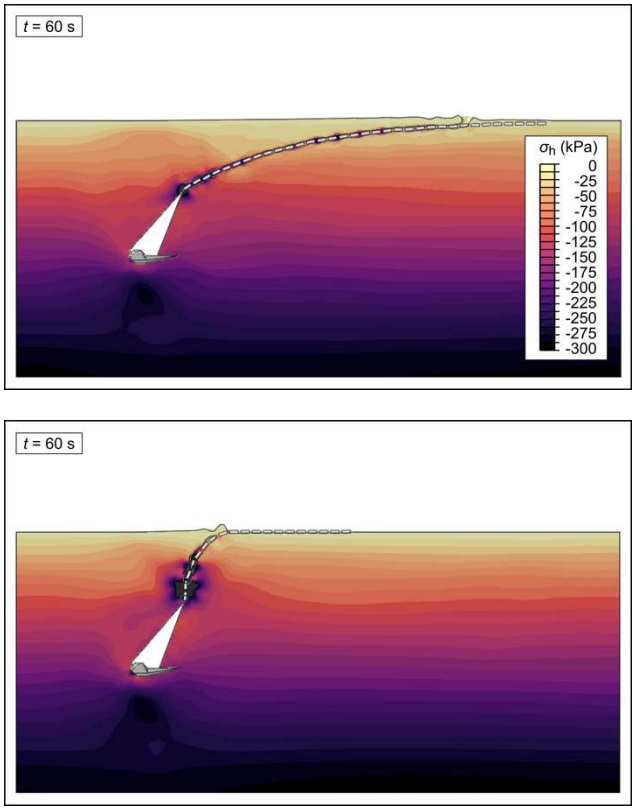

Figure 12. Configuration of anchor chain and stress state (in kPa) of the soil after pulling for different anchor line angles 30 ° (top) and 80 ° (bottom) in simulations 2 and 5.

The most significant differences in displacement occurred at the smallest angle, where the high horizontal load transfer led to minimal vertical lifting of the anchor during cyclic tensile loading, see Fig. 13. Consequently, the soil beneath the anchor was less compacted, resulting in greater negative vertical displacement at this angle. The 60 ° anchor line angle also exhibited the greatest vertical displacement, indicating that it provided the lowest overall resistance in the anchoring system. Conversely, the 30 ° angle displayed the greatest resistance.

4.3 *Impact of initial void ratio*

Figure 14 illustrates the chain configuration and horizontal stress states following operational loading for simulations 3, 6 and 7. The results from both simulations reveal similar stress distributions and anchor chain configurations.

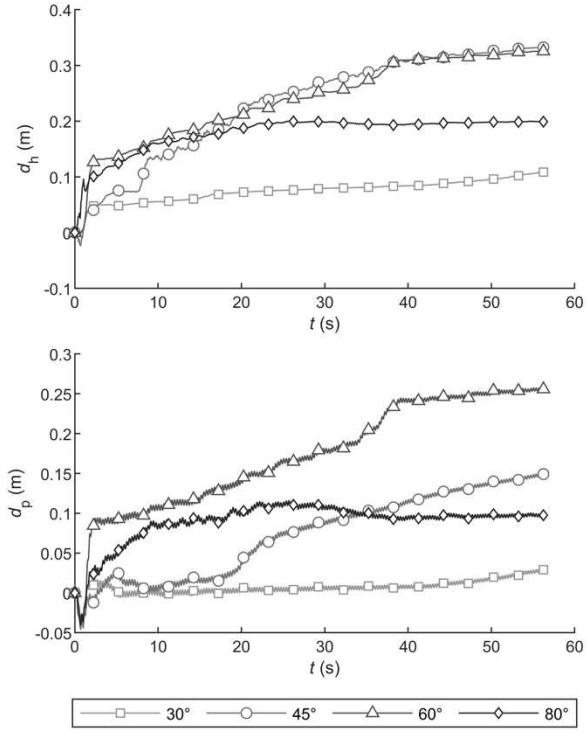

Figure 13. Horizontal (top) and vertical (bottom) displacement d_h and d_p of the anchor fluke tip P_h during loading for different anchor line angles.

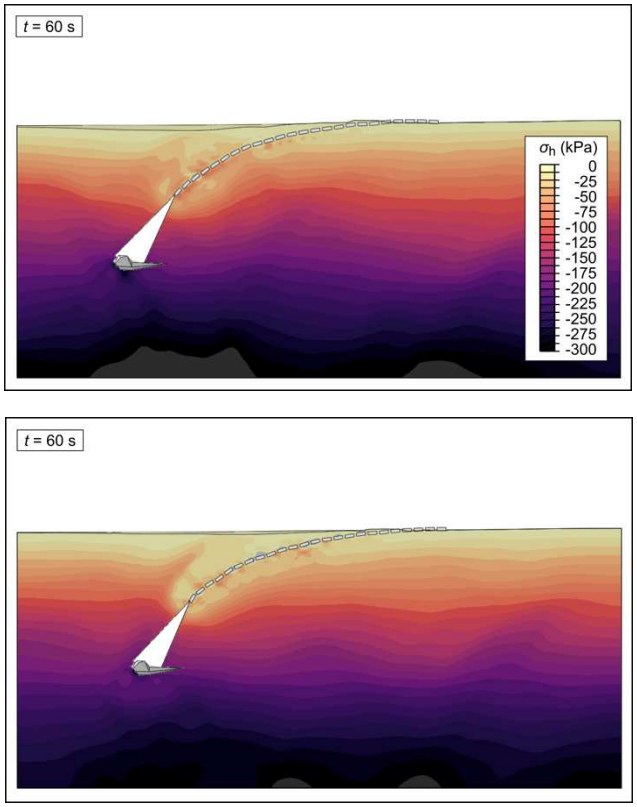

Figure 14. Configuration of anchor chain and stress state (in kPa) of the soil after pulling for different initial void ratios e_{max} (top) and e_{min} (bottom) in simulations 6 and 7.

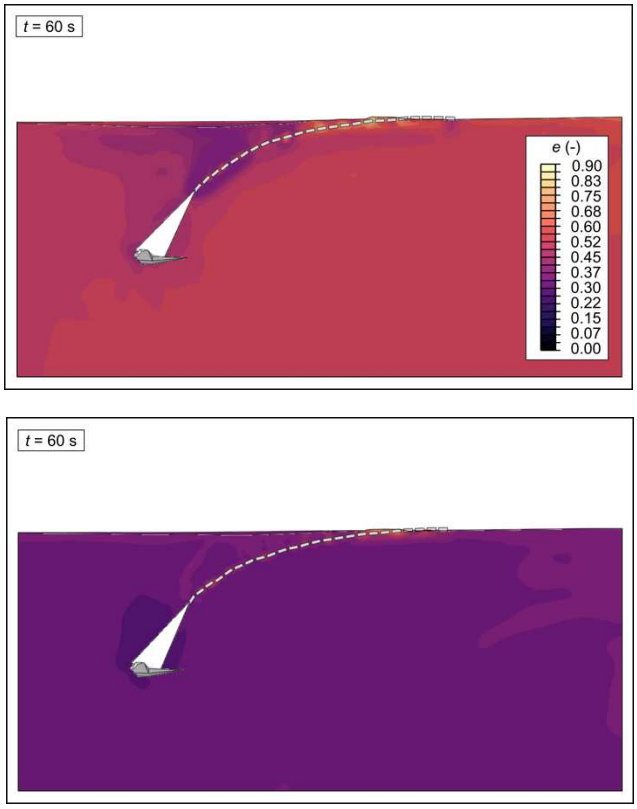

Figure 15. Distribution of void ratio in the soil after pulling for different initial void ratios e_{max} (top) and e_{min} (bottom) in simulations 6 and 7.

Figure 15 depicts the chain configuration and void ratio distribution following operational loading in simulations 6 and 7, showing similar outcomes for both. The cyclic load led to soil compaction during the loading phase, with increased compaction observed near the initial chain links of the anchoring system's connecting piece. This load was transmitted from the chain to the soil through contact, subjecting the nearby soil to similar loads as the anchor chain. Consequently, this interaction resulted in soil loosening directly beneath the anchor chain and further compaction of the soil above this area and below the loosened zone. Variations in stress magnitude across different areas can be attributed to the initial void ratios; areas with lower void ratios experienced higher stresses due to the denser soil structure.

Analysis of anchor displacement revealed that the horizontal displacements at the anchor fluke tip were consistent across different initial void ratios, see Fig. 16. However, there is the exception of the most loosely packed soil, which exhibited a reduction in horizontal displacement from the peak tensile load to the end of the loading phase. In contrast, vertical displacements varied significantly. Soils with smaller initial void ratio, being denser at the start of loading, exhibited lower settlements or vertical displacements. Conversely, soils with a higher void ratio allowed for greater settlement due to their larger pore volume. This increased settlement leads to soil compaction and heightened soil resistance.

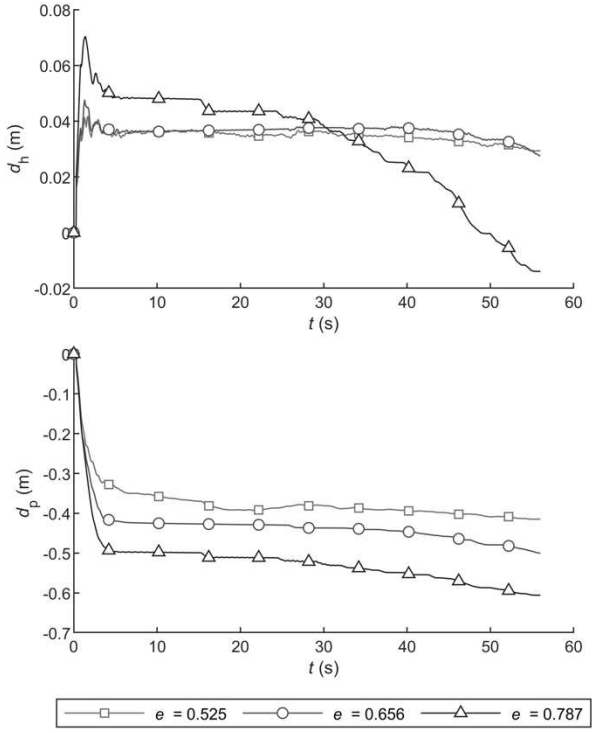

Figure 16. Horizontal (top) and vertical (bottom) displacement d_h and d_p of the anchor fluke tip P_{ft} during loading for different initial void ratios.

5 SUMMARY AND OUTLOOK

This study developed a three-dimensional model to simulate the behavior of a tension-loaded anchor chain within soil. Through comprehensive simulations, the research analyzed the influence of various factors on the anchor chain-soil interaction under operational conditions, with a focus on cyclic loading.

The findings indicate that the Mohr-Coulomb model is less effective in accurately predicting responses to cyclic loading. Conversely, the hypoplastic model offered a more realistic presentation of soil resistance under similar conditions. The parameters for each constitutive model were obtained from different sources. The parameters of the hypoplastic model have undergone verification, while those for the Mohr-Coulomb model are derived from publicly accessible experimental protocols and should be considered preliminary estimates of behaviour. The differences arise from the application of a uniform deformation modulus across all stages in the Mohr-Coulomb simulations. In contrast, the hypoplastic model can accommodate variations in stiffness during simulation. For the design case of an anchor chain, the Mohr-Coulomb model should be used cautiously, providing only a preliminary estimation. In cyclic loading scenarios, it is recommended to employ an increased modulus that more accurately reflects the soil's behaviour under operational conditions.

Comparison to former simulations showed severe difference in the stress distribution, presenting more realistic results, modelling the complete anchor instead of just a mass point.

The results highlighted that cyclic loading induced soil compaction near the initial chain links and caused soil loosening directly below the anchor chain, accompanied by additional soil compaction above the anchor chain and below the loosened area. Soils with lower initial void ratios exhibited higher resistance and increased stresses. In contrast, soils characterized by higher void ratios underwent more substantial settlements, resulting in increased soil compaction and enhanced resistance.

Regarding the impact of the anchor line angle, horizontal displacements of the anchor fluke tip were similar at angles of 45 ° and 60 °, showing significant movement, while displacements at angles of 30 ° and 80 ° were less pronounced. Correspondingly, vertical displacements were also greatest at 45 ° and 60 °.

Further investigations should integrate the anchor installation process with operational state evaluations across all considered material models, allowing initial stress states from the installation to inform subsequent operational analyses. Such integration will provide a more realistic assessment of soil resistance at the onset of operational simulations, crucial for the design and evaluation of floating offshore wind turbines (FOWTs).

The insights gained lay a foundational framework for further research into the mooring system behavior of FOWTs under operational cyclic loading. Continued model refinement and the integration of these simulation results into the FOWT design process could enhance the understanding of anchor chain-soil interactions, promoting safer and more economically viable construction practices for offshore wind installations.

6 ACKNOWLEDGEMENTS

This work was supported by the German Research Foundation (DFG), under Grant GR 1024/61-1. The authors express their gratitude for the financial assistance provided. We also extend our thanks to our students Noah M. H. Coutinho, Kaja Ondruch and Theodore W. Stager for their involvement in the development of the numerical model.

7 REFERENCES

Bienen B., Fan S., Schröder M. and Randolph M. F. 2021. Effect of the installation process on monopile lateral response. *Proceedings of the Institution of Civil Engineers – Geotechnical Engineering* 174 (5), 530-548. DOI: 10.1680/jgeen.20.00219

Benson D. J. 1992. Computational methods in Lagrangian and Eulerian hydrocodes. *Computer Methods in Applied Mechanics and Engineering* 99 (2-3), 235–394.

Cerek K., Dao D. A., Hadjiloo E. and Grabe J. 2024. Dataset of Simulated CRS Tests for Advanced Soil Parameter Identification. DOI: 10.15480/882.9435

Chow S. H., Roy A., Herduin M., Heins E., King L., Bienen B., O'Loughlin C., Gaudin C. and Cassidy, M. J. 2019. Characterisation of UWA superfine silica sand. DOI: 10.26182/5d8c185bcd366

Dao D. A. and Grabe J. 2022. Numerical investigation of ship anchor penetration in cohesive Baltic Sea soil. *Proceedings of the 41st International Conference on Ocean, Offshore and Arctic Engineering*, Hamburg, Germany, V009T10A002. DOI: 10.1115/OMAE2022-80822

Dao D. A. and Dicke K. 2024. Numerical investigation of drag embedment anchor model reduction for FOWTs in coarse and fine-grained Baltic Sea soil. *Proceedings of the 5th International Conference on Geotechnics for Sustainable Infrastructure Development*, Hanoi, Vietnam, e-ISBN: 978-981-99-9722-0.

Dao D. A. and Banduch M. 2023. Geotechnical Laboratory Investigation on the Baltic Sea Sand Sample Z_VC_011. DOI: 10.15480/882.8440

Dao D. A., Alkateeb D. and Schröder M. 2023. Discrepancies between element tests and large-scale LDFE simulations: a case study on anchor kinematics during installation in clay. *Computers and Geotechnics* 163, 105698. DOI: 10.1016/j.compgeo.2023.105698

Dao D. A., Struve A. and Grabe J. 2022a. Numerical Investigation on the Effect of Anchor Modelling on Anchor Chain-Soil Interaction for Floating Offshore Wind Turbines. *Proceedings of the 15th International Symposium on Practical Design of Ships and other Floating Structures*, Dubrovnik, Croatia, 1673-1684 , ISBN 978-953-7738-87-7.

Dao D. A., Dicke K. and Grabe J. 2022b. Investigation of anchor installation for floating offshore wind turbines. *Proceedings of 10th International Conference on Physical Modelling in Geotechnics*, Daejon, Korea, 482-485, ISBN: 978-89-952197-7-5.

Dao D. A. and Grabe J. 2024. Modeling the interaction between ship anchors and cables in Baltic Sea soils. *Proceedings of the 17th Pan-American Conference on Soil Mechanics and Geotechnical Engineering*, La Serena, Chile.

Dassault Systèmes. 2020. *Abaqus documentation*.

Degenkamp G. and Dutta, A. 1989. Soil Resistances to Embedded Anchor Chain in Soft Clay. *Journal of Geotechnical Engineering* 115 (10), 1420–1438. DOI: 10.1061/(asce)0733-9410(1989)115:10(1420)

Herle, I. and Gudehus G. 1999. Determination of parameters of a hypoplastic constitutive model from properties of grain assemblies. *Mechanics of Cohesive-frictional Materials* 4 (5), 461–486.

Kim Y. H. and Hossain M. S. 2015. Dynamic installation of OMNI-max anchors in clay: Numerical analysis. *Géotechnique*, 65 (12), 1029-1037. DOI: 10.1680/jgeot.15.T.008

Kwa K., Festa O. G., White D., Sobey A. and Gourvenec S. 2023a. Design benefits for plate anchors for floating offshore wind through coupling floater, mooring and geotechnical responses. *Proceedings of the 9th International SUT OSIG Conference "Innovative Geotechnologies for Energy Transition"*, London, United Kingdom, 1196-1203.

Kwa K., Festa O. G., White D., Sobey A. and Gourvenec S. 2023b. Integrated numerical modelling of soil-anchor-mooring line-floater response for floating offshore wind. *Proceedings of the 10th European Conference on Numerical Methods in Geotechnical Engineering*, 1-6. DOI: 10.53243/NUMGE2023-129

Machaček J., Brosz F., Staubach P., Wichtmann T., Zachert H. 2022. Back-calculations of Centrifuge Tests on Pile Groups Subjected to High-cyclic Loading. *International Conference on Deep Foundations and Ground Improvement: Smart Construction for the Future*, Berlin, Germany, 534-544.

Maitra, S., Tian, Y. and Cassidy, M. J. 2022. Investigation of the installation process of drag-in plate anchors from LDFE modelling. *Géotechnique*, Ahead of Print. DOI: https://doi.org/10.1680/jgeot.21.00402

Neubecker S. and Randolph M. F. 1995. Profile and frictional capacity of embedded anchor chains. *Journal of Geotechnical Engineering*, 121 (11), 797–803.

Noh, W. F. 1963. *CEL: A time-dependent, two-space-dimensional, coupled Eulerian-Lagrange code.* Lawrence Livermore National Lab, Livermore, California, United States.

O'Neill M. P., Erbrich C. and McNamara A. 2018. Prediction of Seabed Trench Formation Induced by Anchor Chain Motions. *Proceedings of the Offshore Technology Conference*, Houston, Texas, USA. DOI: 10.4043/29068-ms

O'Neill M. P., Bransby M. F. and Randolph M. F. 2003. Drag anchor fluke-soil interaction in clays. *Canadian Geotechnical Journal* 40 (1), 78–94. DOI: 10.1139/t02-096

Stapelfeldt M., Alkateeb D., Grabe J. and Bienen B. 2020. Numerical simulation of cone penetration tests inside suction caisson foundations in sand. *Proceedings of the 39th International Conference on Offshore Mechanics and Arctic Engineering*, V010T10A007. DOI: 10.1115/OMAE2020-18721

Sun C., Feng X., Neubecker S. R., Randolph M. F., Bransby M. F. and Gourvenec S. 2019. Numerical study of mobilized friction along embedded catenary mooring chains. *Journal of Geotechnical and Geoenvironmental Engineering*, 145 (10), 1–13.

Wang L.-Z., Guo Z. and Yuan, F. 2010. Three-dimensional interaction between anchor chain and seabed. *Applied Ocean Research* 32 (4), 404–413. DOI: 10.1016/j.apor.2010.09.001

Vivatrat V., Valent P. J. and Ponterio A. A. 1982. The influence of chain friction on anchor pile design. *Proceedings of the Offshore Technology Conference*, Houston, Texas, USA. DOI: 10.4043/4178-MS

von Wolffersdorff, P.-A. 1996. A hypoplastic relation for granular materials with a predefined limit state surface. *Mechanics of Cohesive-frictional Materials: An International Journal on Experiments*, Modelling and Computation of Materials and Structures, 1 (3), 251–271.

Vryhof. 2021. History of anchors. https://vryhof.com/news/vryhof-history-of-anchors/, accessed on May 14th 2021.

Vryhof. 2018. *Vryhof Manual: the Guide to Anchoring*.

Xiong L., Yang J. and Zhao W. 2016. Dynamics of a taut mooring line accounting for the embedded anchor chains. *Ocean Engineering* 121, 403–413. DOI: https://doi.org/10.1016/j.oceaneng.2016.05.011

Zhao Y. and Liu H. 2016. Numerical implementation of the installation/mooring line and application to analyzing comprehensive anchor behaviors. *Applied Ocean Research*, 54 (5), 101–114.

Zienkiewicz O. C., Taylor R. L. and Zhu J. Z. 2005. *The finite element method: its basis and fundamentals*. 6th Edition.